International Journal of Medical, Medicine and Health Sciences
ISSN: 2517-9969
Vol:11, No:11, 2017

Scattering Operator and Spectral Clustering for Ultrasound Images: Application on Deep Venous Thrombi

Thibaud Berthomier, Ali Mansour, Luc Bressollette, Frédéric Le Roy, Dominique Mottier, Léo Fréchier, Barthélémy Hermenault

***Abstract*—**Deep Venous Thrombosis (DVT) occurs when a thrombus is formed within a deep vein (most often in the legs). This disease can be deadly if a part or the whole thrombus reaches the lung and causes a Pulmonary Embolism (PE). This disorder, often asymptomatic, has multifactorial causes: immobilization, surgery, pregnancy, age, cancers, and genetic variations. Our project aims to relate the thrombus epidemiology (origins, patient predispositions, PE) to its structure using ultrasound images. Ultrasonography and elastography were collected using Toshiba Aplio 500 at Brest Hospital. This manuscript compares two classification approaches: spectral clustering and scattering operator. The former is based on the graph and matrix theories while the latter cascades wavelet convolutions with nonlinear modulus and averaging operators.

***Keywords*—**Deep venous thrombosis, ultrasonography, elastography, scattering operator, wavelet, spectral clustering.

I. Introduction

IN normal conditions, a thrombus is formed to stop bleeding in case of injuries [1]. This natural process, called clotting, locally changes blood to a gel, thrombus, and lasts until the injured vessel is healed. This natural process is normally followed by a fibrinolysis step to dissolve the existing thrombus. However, this last step may be deficient or a thrombus may occur in an inappropriate situation (without the presence of bleeding).

An abnormal thrombus in deep venous network of the leg is named Deep Venous Thrombosis (DVT). Less known than myocardial infarction or cardiovascular diseases, DVT may also have deadly consequences. Indeed, a piece or the entire thrombus could break off, be carried by the blood to the lung and cause a Pulmonary Embolism (PE). In Europe, DVT and PE affect respectively about 680 and 430 thousand individuals per year [2].

Although DVT can be detected using ultrasound, this disease is still difficult to diagnose at an early stage. In fact, DVT is often clinically silent and, in many cases, the first sign of the disease is an intense pain in the leg or a sudden PE. DVT is a multifactorial disease [1] involving interactions among clinical risk factors (extended immobilization, surgery, age, etc.) and predispositions to thrombosis (cancer, genetic mutation, hormone, pregnancy, etc.).

The purpose of our project is to correlate the triggering factors of the DVT, the presence of PE and the gelatinous structure of the thrombus. Two ultrasound imaging techniques are considered to visualize the thrombi: ultrasonography and elastography. The two techniques highlight respectively the thrombus echogenicity and its stiffness. More details about these imaging techniques and the database are provided in Section II.

To characterize the thrombus structure, this manuscript considers two approaches: scattering operator and spectral clustering. Both algorithms, explained in Section III, are aiming to extract discriminative information from ultrasound images. Section IV describes the simulation procedure and discusses the obtained results.

Thibaud Berthomier is with the LABSTICC (UMR 6285), ENSTA Bretagne, 29200 Brest, France and EA 3878 (GETBO), CIC Inserm 1412, CHU de la Cavale Blanche, 29200 Brest, France (corresponding author, e-mail: thibaud.berthomier@ensta-bretagne.org).

Ali Mansour and Frédéric Le Roy are with the LABSTICC (UMR 6285), ENSTA Bretagne, 29200 Brest, France.

Luc Bressollette, Dominique Mottier, Léo Fréchier and Barthélémy Hermenault are with the EA 3878 (GETBO), CIC Inserm 1412, CHU de la Cavale Blanche, 29200 Brest, France.

II. Deep Venous Thrombus Imaging

This section explains how a thrombus can be detected and observed using ultrasound imagery techniques: ultrasonography in Subsection II-A and elastography in Subsection II-B. Then, Subsection II-C described our database and the acquisition process.

A. Ultrasonography

Ultrasonography is a common approach to diagnose a DVT. Using ultrasonography, physicians can observe the blood network, view the blood flow and check on the veins compressibility. A vein with a blood clot is relatively incompressible and is more echogenic than a free vein. In comparison with other techniques (Contrast venography, Magnetic Resonance Angiography or Computed Tomography Angiography) [3], ultrasonography may have a lower quality image but it is direct, cheap, less-time-consuming, repeatable and non-invasive.

At the beginning of a DVT episode (in the first hours or days), the clot is hypoechoic, homogeneous, elastic and it dilates the vein. On the contrary, an older clot (several weeks) becomes slowly more heterogeneous, harder and smaller. The clot echogenicity actually depends on the blood cell composition, distribution and its fibrin mesh. The exact age of the thrombus can help determining the right treatment (anticoagulant, surgery). The study presented in [4] tries to

age thrombi by characterizing their echostructure. However, the authors of [5], [6] outcome more promising results to date the thrombus with a more recent ultrasound imaging technique named elastography.

B. Elastography

Elastography consists in mapping the hardness, or the elasticity, of human tissues: the harder a tissue is the more elastic it becomes. Human soft tissues can distort under the influence of two types of mechanical waves: compressional and shear waves. Ultrasonography systems emit compressional waves and analyze their echoes to build the image. By contrast, elastography is obtained by estimating the shear wave velocity through the tissue. Indeed, their velocity is linked to the tissue elasticity E by

$$E = 3\rho c^2 \tag{1}$$

where ρ is the volume density (kg/m^3) and c the shear wave velocity (m/s) [7].

Nowadays, elastography is extensively investigated in many potential applications such as: liver fibrosis staging, thyroid, lymph node, pancreas and breast cancer diagnosis [7]. As aforementioned, several studies like [5] and [6] create an animal model to estimate the exact age of the venous thrombus in vivo using ultrasonography. On human patients, the thrombus real age is difficult to be estimated because patients normally consult their doctor after the first signs (intense pain or PE) or when they have a high probability of DVT (cancer). Thus, in our study cases, the blood clot can have between 3 days and two weeks. However, elastography can give information on the thrombus structure.

C. Data Acquisition Process and Database

In the case of a DVT suspicion, the physician locates the thrombus head using compression ultrasonography. At Brest Hospital, Toshiba Aplio 500 systems are used to diagnose DVT using ultrasonography and elastography. After switching to the elastography mode, the physician can select a Region Of Interest (ROI). For an existing obstacle (such as a tumor in the tissue or a clot in a vein), the shear wave velocity in that area should be different from the velocity of surrounded areas.

The Toshiba system displays the elastography on the left side of the screen and the ultrasonography on the right side. Later on, a physician selects a shape (like an ellipse) around the thrombus shown in the ultrasound image. The shear wave velocity mean and standard deviation in this area are evaluated. The obtained values are called elastometry.

For each patient, transverse and longitudinal measures are collected in our database (see Fig. 1). Each measure contains several acquisitions (e.g. with or without the ellipse). Further details on the acquisition system and process can be found in our previous manuscript [8].

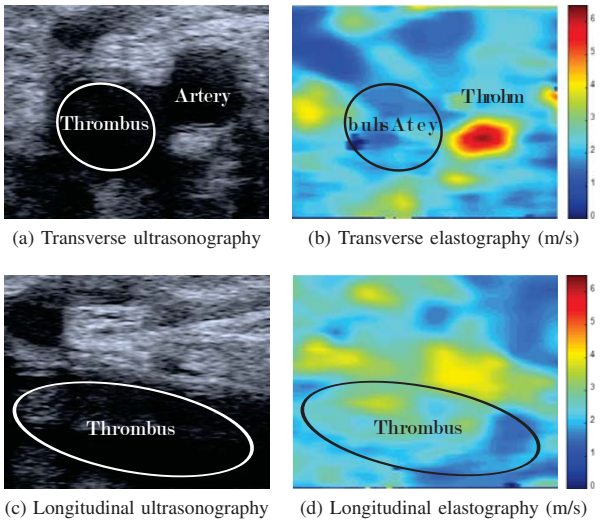

(a) Transverse ultrasonography (b) Transverse elastography (m/s)

(c) Longitudinal ultrasonography (d) Longitudinal elastography (m/s)

Fig. 1 Transverse and longitudinal ultrasonographies and elastographies (speed map) of a thrombus in the femoral vein (images obtained with Toshiba Aplio 500)

III. Feature Extraction and Classification

In order to characterize the thrombi structure with ultrasound images (ultrasonography and elastography), two approaches, explained in Subsections III-B and III-C, are considered in this manuscript: Scattering Operator(SO) and Spectral Clustering (SC). Subsection III-A presentes the preprocessing steps computed upstream the feature extraction and the classification.

A. Preprocessing

Our database contains DICOM files composed of a screenshot image and metadata. First, the acquisition parameters, the orientation of the view (transverse, longitudinal) and the epidemiology of the patient (thrombus head localization, triggering factors, age, PE) are recovered and stored in a file. Then, the ultrasonography and the elastography are extracted from the screenshot image based on the ROI highlighted by the physician (see Fig. 1).

During the medical examination, the physician often needs to adjust some parameters to observe the blood clot. To standardize our acquisition, we propose the equalization of obtained histograms with Contrast-Limited Adaptive Histogram Equalization (CLAHE) [9] which performs histogram equalization over each region of the image using a transformation function (e.g. Rayleigh distribution). The slope associated with the gray level assignment function is limited by a threshold to avoid the overamplification of small amounts of noise in a large homogeneous region. As shown in Fig. 2, CLAHE improves the local contrast and enhances the definitions of edges.

Finally, to characterize only the thrombus and optimize the scattering operator computation, a square image, as big as possible, is extracted inside the drawn ellipse. The square size differs according to the patient (its anatomy), the clot age, its size and its localization (vein). The scattering operator technique requires that the input images should have the same size. In this manuscript, the images are resized using zero padding in the discrete cosine transform at the size 64×64

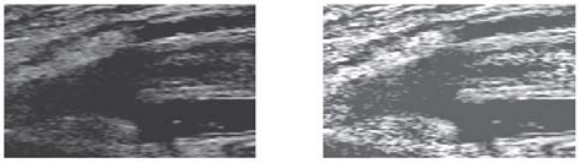

(a) Before CLAHE (b) After CLAHE

Fig. 2 Longitudinal ultrasonography before and after Contrast-Limited Adaptive Histogram Equalization (CLAHE) [9] (images obtained with Toshiba Aplio 500)

pixels (about the median value of the sizes of all the extracted images). Our preprocessing steps are available in a previous manuscript [10].

B. Scattering Operator

An ultrasound image often presents as textured areas with organs, tumors, vessels, etc. The textured areas are non-homogenous in appearance as they suffer from small local deformations due to the characteristics of the human tissues and the image acquisition process. The key idea is to build a new representation where the high variability within a same class of images is reduced. One possible approach is to consider the Scattering Operator (SO) which provides a representation that is invariant to global translations and specifically stable to local deformations [11]. This operator shows promising results to classify synthetic textured images [12] but also sonar images of seabed [13].

A scattering transform convolutes the input images with dilated and oriented wavelets which are obtained by rotating and scaling of a mother wavelet Ψ by $\theta \in \Theta$ angles and by $j \in [0, J]$ scales:

$$\Psi_{j,\theta}(u) = 2^{-2j}\Psi(2^{-j}r_\theta^{-1}u) \tag{2}$$

where $u \in \mathbb{R}^2$ stands for the spatial position vector and the rotation matrix is given by

$$r_\theta = \begin{pmatrix} \cos\theta & -\sin\theta \\ \sin\theta & \cos\theta \end{pmatrix}. \tag{3}$$

In the simulations described Section IV, Ψ is a Morlet wavelet [11] which is a complex wavelet composed of a complex exponential multiplied by a Gaussian window.

Wavelets are localized waveforms stable to small deformations but they are translation variant. The invariance can be obtained with a complex modulus and a local averaging. The averaging is obtained using a low pass-filter Φ:

$$\Phi_J(u) = 2^{-2J}\Phi(2^{-J}u) \tag{4}$$

where 2^J is the maximum scale and Φ is a scaling function called the father wavelet. In our simulations, Φ is selected as a rotationally invariant Gaussian [11]. The directional wavelet transform vector of an image x at position u ($\star$ is a convolution product) is defined by :

$$W_J x(u) = \{x \star \Psi_{j,\theta}(u), x \star \Phi_J(u)\}_{j<J,\theta\in\Theta}. \tag{5}$$

The image average $S[\emptyset]x$ defines the first coefficient of the scattering transform of x:

$$S[\emptyset]x = x \star \Phi_J. \tag{6}$$

where $\emptyset$ means that no scale j or orientation θ are used to computed $S[\emptyset]x$.

The averaged wavelet coefficients $S[j_1, \theta_1]x$, obtained for each scale $j_1 < J$ and each orientation $\theta \in \Theta$, form the first order coefficients:

$$S[j_1, \theta_1]x = |x \star \Psi_{j_1,\theta_1}| \star \Phi_J. \tag{7}$$

It is worth mentioning that the averaging reduces the high frequency information so the scattering operator recovers the lost in high frequencies by applying a convolution with wavelets Ψ_{j_2,θ_2} at scales $j_2 < J$ and orientations $\theta_2 \in \Theta$. The convolution with Ψ_{j_2,θ_2} give co-occurrence coefficients for any pair of scales 2^{j1}, 2^{j2} and any two orientations θ_1 and θ_2. These two levels of decomposition can be used to distinguish corners and junctions from edges. To make these co-occurence coefficients translation invariant, another modulus and another averaging process are again applied:

$$S[(j_1, \theta_1), (j_2, \theta_2)]x = ||x \star \Psi_{j_1,\theta_1}| \star \Psi_{j_2,\theta_2}| \star \Phi_J \tag{8}$$

$S[(j_1, \theta_1), (j_2, \theta_2)]x$ are named the ordre-2 coefficients.

Further iterations on the wavelet transforms and the modulus operators enable evaluating more translation invariant coefficients. A scattering transform aggregates all these coefficients up to a maximum order M. For a large invariant representation, several layers are necessary to avoid losing crucial information. The number of rotations, scales and layers are key parameters of the scattering transform and need to be optimized.

C. Spectral Clustering

Recently, Spectral Clustering (SC) [14], [15] is one of the most widely used techniques for exploratory data analysis in many applications related to machine learning, computer vision and/or signal processing. The key idea of clustering is to divide a dataset into similar groups. The algorithm presented in [15] shows promising results for ultrasound segmentation [16] and brain Magnetic Resonance Imaging segmentation [17]. In our case, the objective is not to classify pixels within an image (i.e. segmentation) but to classify the image themselves. Therefore, our images are reshaped into vectors before applying this algorithm.

The first step consists to build a similarity matrix W to evaluate the resemblance among the image vectors x_i of our database composed of n images. Each couple (x_i, x_j) is associated with a similarity value w_{ij}. Similarity matrix W is then composed of terms w_{ij} which can be of cosine, fuzzy or Gaussian types. In this manuscript, the most used Gaussian type is considered and defined by:

$$w_{ij} = exp\left(-\frac{d^2(x_i, x_j)}{2\sigma^2}\right) \tag{9}$$

where σ is the scaling parameter of the Gaussian function and $d(x_i, x_j)$ stands for the Euclidean distance between x_i and x_j.

The second step is the construction of a weighted graph G where the edge connecting two points is weighted by their similarity value. There are several ways to build a graph (fully connected, r-neighborhood, k-nearest neighbor) [14]. In our study, fully connected graphs are considered to estimate the similarities of each sample without a priori knowledge.

Many methods can then be used to cut the graph into K clusters. The main objective is to minimize the weights (or similarities) assigned to the removed edges. An efficient approach is to use the Jordan and Weiss Spectral Clustering (JWSC) algorithm [18]:

1) Construct the graph and the similarity matrix W representing the dataset (as defined previously).
2) Compute the normalized Laplacian L:
$$L = D^{-1/2}(D - W)D^{-1/2} \tag{10}$$
where $D \in \mathbb{R}^{n\times n}$ is a diagonal matrix, called degree matrix, having on its diagonal the elements d_i:
$$d_i = \sum_{j=1}^{n} w_{ij}. \tag{11}$$
3) Find the K first eigenvectors of L and form the matrix U by stacking the eigenvectors in columns to obtain a lower-dimensional representation.
4) Get the matrix T from U by normalizing each of Us rows:
$$T_{ij} = U_{ij}\left(\sum\nolimits_{j=1}^{n} U_{ij}^2\right)^{-1/2} \tag{12}$$
5) In the new representation, classify each row of T into K clusters using K-means algorithm or another classification algorithm.
6) Label the original point x_i to the cluster of the corresponding row i of T.

At the end of the JWSC algorithm, the database is classified into K clusters whose label number ($[1, 2...K-1, K]$) depends on the K-means initialization. The classification results presented in Subsection IV-B are computed after permutation of the labels in order to get the best rate. The two approaches (SO and SC) are compare by applying a K-means algorithm directly on the scattering transforms.

IV. Simulations

Our project aims to extract thrombi structure features and to link them to patients' epidemiology. This manuscript considers two approaches to extract features and classify our ultrasound images:

1) Scattering Operator (SO)
2) Spectral Clustering (SC)

As explained in Subsection II-B, the SO parameters (number of scales, orientations and orders) should be optimized. However, this optimization step is difficult to carry out on our ultrasound database for three main reasons:

- The size of our database: around 19 patients with a total of almost 100 images;
- The patient epidemiology and the thrombus structure may not be correlated;
- The cause to effect relationship may not be highlighted with ultrasonography and elastography.

For the selection of the SO parameters, we suggest in Subsection IV-A to apply the SO on a richer and more consistent database which contains synthetic textured images. In the Subsection IV-B, we evaluate the performances of the two developed approaches (SO and SC) on this synthetic textured database. Then, Subsection IV-C describes our simulation results on our ultrasound images.

A. Scattering Operator Optimization

The scattering operator can be adjusted and tuned by changing some key parameters such as the numbers of scales J, orientations L and orders M. The authors of [19] suggest the use of 8 orientations ($L = 8$), at least 2 orders ($M = 2$) and J scales with J defined by:
$$J = \frac{log_2(N)}{2} - 2 \tag{13}$$
where N is the total number of pixels in the image. With an image containing 128×128 pixels, J will be equal to 5.

As aforementioned, the parameter optimization is not realized directly on our ultrasound database but rather on a synthetic textured database called KTH-TIPS [20] (KTH is the abbreviation of the authors' university, and TIPS stands for Textures under varying Illumination, Pose and Scale). This database was created by providing variations in scale, pose and illumination of ten materials (see Fig. 3). Each class contains 81 small images (128×128 pixels) which are converted to grayscale images for the described simulations.

In order to select the parameters (J, L and M) and to compare our results to the ones in [12], we suggest to compute supervised classification. Generally, supervised classifier conducts to divide our database into two sets: the training and the test sets. As a scattering representation linearizes the small deformations [11], an affine space model classifier is well-adapted. In our simulations, the affine space is computed with a Principal Component Analysis (PCA). The PCA diagonalizes the covariance of the scattering transform S. Then, k covariance eigenvectors of largest variance are selected to generated the space model of each class. k is called the dimension of the generated affine space. Finally, each test image is assigned to the closest model (*i.e.* class). The dimension k can be adjust by a cross validation with the SO parameters J, L and M: the scattering operator and PCA are computed for several J, L, M and k and the set of parameters which gives the best classification rate is selected [11].

For the cross validation procedure, we computed the scattering transforms on the textured images for several set of parameters noted by:

- Scales J: 2, 3, 4, 5, 6 and 7;
- Orientations L: 1, 2, 4, 6 and 8;
- Orders M : 1, 2 and 3

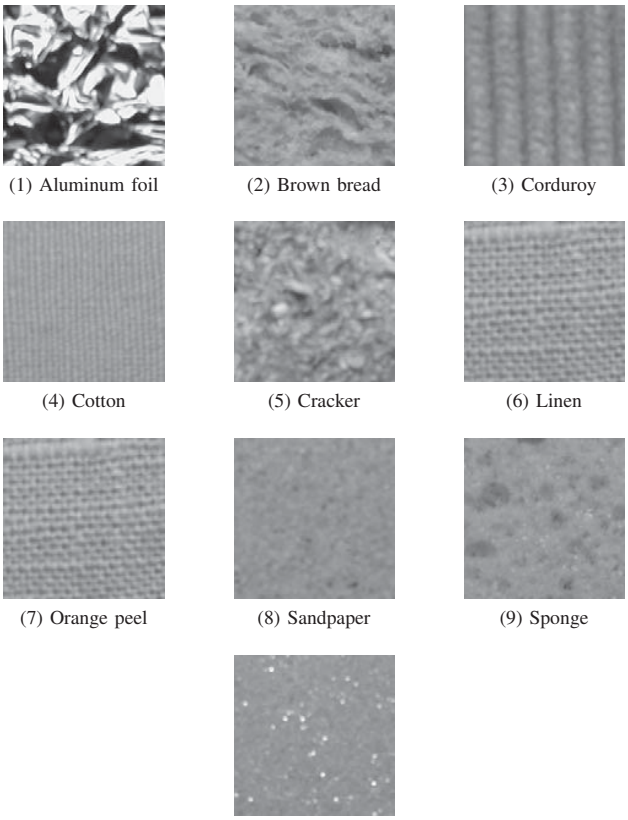

Fig. 3 Images of the materials present in the KTH-TIPS database [20]

The cross validation procedure (results none reported here) justifies the selection of the parameters $J = 5$ and $L = 8$ and highlights that $M = 2$ is already enough to obtain excellent results.

Tables I gives the classification rates with those parameters and over 200 random splits (training/test) of KTH-TIPS. According to the cross validation procedure, k is defined as the number of images in the training set. SO performances are compared to those of three methods described and applied in [12]: Log Gaussian Cox processes (COX) [21], Basic Image, Features (BIF) [22] and Sorted Random Projection (SRP) [23]. COX gives better classification rates with a small training set (5 images) but lower rates with a more important training set (20 or 40 images). SO, BIF and SRP have similar performance (around 98%) with important training sets (40 training images). Our simulations with the SO produce very similar results to [12].

However, as suggested by the authors of [12], the SO performance can be improved by applying the PCA on the logarithm of the scattering coefficients (see row "SO + log" in Table I). The logarithm linearizes the exponential decrease of the scattering coefficient energy among each orders [11]. To improve the performance of the SO with a small training set, one can scale the size of the training set by a power of 2 each scattering vector of the training set. This method, called

TABLE I
CLASSIFICATION RATES WITH STANDARD DEVIATIONS ON KTH-TIPS DATABASE FOR THREE TRAINING SIZES PER CLASS: THE FIRST FOUR ROWS GIVE THE RESULTS PUBLISHED IN [12] AND THE LAST THREE ROWS GIVE OUR SIMULATION RESULTS

Train size	5	20	40
COX [21]	80.2 ± 2.2	92.4 ± 1.1	95.7 ± 0.5
BIF [22]	-	-	98.5
SRP [23]	-	-	99.3
SO [12]	69.1 ± 3.5	94.8 ± 1.3	98.0 ± 0.8
SO	68.8 ± 3.96	96.2 ± 1.1	99.0 ± 0.6
SO + log	75.5 ± 3.6	96.8 ± 1.2	99.1 ± 0.6
SO + log + MT	79.7 ± 3.3	96.9 ± 1.0	98.9 ± 0.7

TABLE II
CLASSIFICATION RATES WITH STANDARD DEVIATIONS ON KTH-TIPS DATABASE FOR UNSUPERVISED CLASSIFICATION

Methods	Mean and Standard deviation
SO	39.6 ± 2.1
SO + log	48.2 ± 3.9
SC	44.0 ± 3.9

Multi training (MT), combined with logarithm makes the SO as performing as COX with 5 training images per class (see row "SO + log + MT" in Table I). Therefore, this methode can so be interesting when the size of our ultrasound database will become large enough for supervized classification.

B. Scattering Operator and Spectral Clustering Comparison

The previous Subsection describes how we selected the SO parameters (L, J and M) using supervised classification. However, the objective is to classify the thrombi images but, with the current database (small and uncertain classes), we propose in this manuscript two unsupervised approach:

- Scattering operator followed by a K-means;
- Spectral clustering with the JWSC algorithm.

This Subsection evaluates the performance of the two developed approaches (SO and SC) on the KTH-TIPS database. Table II shows the mean and the standard deviation classification rates computed over 10 simulations. On the presented simulations, SC outperforms "normal" SO but the use of the logarithm makes the SO more performing.

Table III gives the confusion matrices of the simulations with the SC and with the SO followed by a logarithm. Each row of the confusion matrix corresponds to an actual class while each column represents the classes predected by the classifer [24]. We can see that six classes are satisfactorily classified (aluminum, brown bread, cracker, linen and styrofoam). Applying the two approaches on only those six classes increase the classification rates to 72.43% (respectively $63,17\%$) with the "SO + log" (resp. the SC).

Three classes are correctly classified with the spectral clustering (aluminum, corduroy and linen). Simulations focus on those three classes improve the performance to 90.1% (resp. 78.07%) for the SC (resp. the "SO + log"). On the contrary, three classes are very misclassified (cotton, sandpaper and sponge) and considering only those three classes do not increase the classification rate (49.8% for "SO + log" and 46.6% for the SC). The most confused classes still remain undistinguishable.

TABLE III
MEAN CONFUSION MATRICES OVER 10 SIMULATIONS

(a) SCATTERING OPERATOR AND LOGARITHM

	1	2	3	4	5	6	7	8	9	10
1	**95**	0	0	0	0	0	0	5	0	0
2	0	**53**	0	0	34	0	0	0	13	0
3	0	4	42	11	3	17	12	0	4	6
4	0	0	13	38	0	15	3	12	3	16
5	12	11	0	0	**58**	0	0	0	19	0
6	0	2	0	0	0	**50**	5	5	1	36
7	0	12	10	1	0	0	**59**	5	6	5
8	0	3	0	17	0	15	13	17	2	33
9	0	28	1	5	6	5	36	6	11	2
10	0	2	0	1	0	19	5	15	0	**58**

(b) SPECTRAL CLUSTERING

	1	2	3	4	5	6	7	8	9	10
1	**93**	4	0	0	1	2	0	0	0	0
2	11	36	25	1	0	13	0	8	5	0
3	0	4	**66**	1	0	14	0	12	3	0
4	0	1	2	17	0	23	0	12	23	22
5	7	10	1	10	40	20	0	8	3	0
6	0	1	1	2	0	**51**	25	2	7	10
7	0	8	2	1	1	0	44	6	6	32
8	0	3	9	16	0	2	0	25	26	19
9	0	1	22	16	1	11	0	18	31	0
10	0	0	3	10	0	10	0	13	27	36

C. Application on Thrombi Images

A reduced database is selected in our recent study with images having similar parameters. A patient, Pi, is represented by one or two couple of transverse and longitudinal ultrasound images. The reduced database contains 8 patients that should be classified according to the DVT origin or/and the presence of PE. We have four patients with cancer, including one who has contracted a PE. One patient gets a DVT and a PE due to an immobilization. Our database contains also two patients with a PE, without clear triggering factors, but with genetic predisposition. The last patient of the database contracts a DVT with unknown cause, which is called idiopathic DVT.

In previous studies [10], [25], the scattering operator was only applied on ultrasonography. However, both ultrasonography and elastography are recently considered. The Scattering Operator (SO) and then the Spectral Clustering (SC) are applied and compared. SO parameters are selected by taking into account the parameter optimization described in Subsection IV-A ($M = 2$, $L = 8$, $J = 4$ and logarithm of the scattering coefficients). Whatever the approach, the classification step is made with the K-means algorithm with K in range of 2 to 5. Transverse and longitudinal views are simultaneously considered. The scattering transforms of each view are combined to form a single vector before applying K-means. For spectral clustering, the two images are fused upstream.

Figs. 4a and 4b show the classification results with respectively the scattering operator and spectral clustering applied on the ultrasonographies. With both approaches, the patients with genetic predisposition ($P6$ and $P7$) are not in the same class, independently from the number of clusters. Spectral clustering classifies the four patients with a cancer in the same class (in two and three clusters) whereas the scattering operator dispatches them into two or three classes. The presence of PE seems to be not related with the thrombus echogenicity: there are often patients with PE in each cluster. However, we can see similarity between SO and CS clusters: $P6$, $P1$ and $P4$ form mostly a same class; the two couples of $P7$ images are in the same class too.

The classification results with elastographies (see Figs. 4c and 4d) do not show real correlation between the thrombus stiffness and the patient epidemiology. As previously, patients with cancer are dispatched in different clusters. The patients with genetic predisposition ($P6$ and $P7$) are classified within a same class with the SO. SC clusters seem to be less stable than SO clusters with elastography ($P3$, $P8$ and $P4$ are not always classified in the same classes).

Furthermore, the different classification results between ultrasonographies and elastographies could suggest that the echostructure and the stiffness of the thrombus are not correlated. In further simulations, ultrasonography and elastography are combined, transverse and longitudinal images are also classified separately but the similar results are observed. A major drawback of our study can be explained by the small size of the available (up to now) reduced database.

V. CONCLUSION

DVT is a major public-health problem, with about half a million DVT events including a third of a million PE events per annum in Europe. This multifactorial disease is often asymptomatic and can also occur with no obvious causes. DVT can progress to more life-threatening PE. Our project is looking to correlate DVT causes, PE appearance and the thrombus structure.

In this manuscript, we describe and implement two approaches (scattering operator and spectral clustering) to characterize a thrombus using ultrasonography and elastography. In order to tune the various parameters required in each approach, we evaluate the two approaches on a synthetic textured database. The previously described simulations show that the scattering operator can achieve excellent performance with supervised classification (about 98% with principal component analysis). The two unsupervised approaches (scattering operator with K-means and spectral clustering) gives satisfactory results (almost 50%). However, the scattering operator outperforms the spectral clustering on the synthetic textured database (respectively 44.0% and 48.2%).

On the thrombi database, whatever the approaches, scattering operator or spectral clustering, the obtained classification results seem to be not related to the DVT epidemiology. However, the major limitation of these experimentations is the small size of the database. Currently, we are looking to increase the size of our database and to assess these methods on salivary gland to help the diagnosis of the Gougerot-Sjgren syndrome. In our future works, we are planning to consider other classification techniques mainly based on statistics approaches such as support vector machine or deep learning.

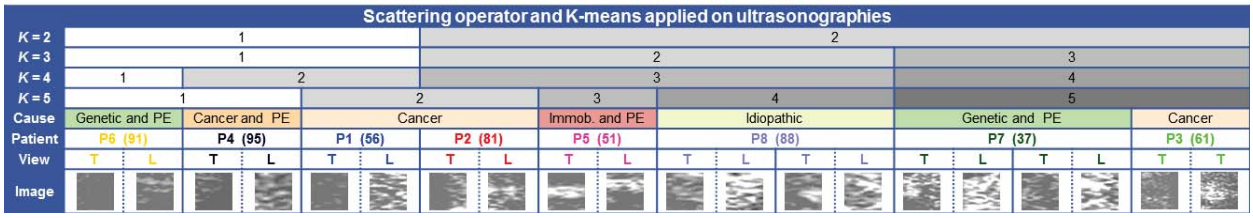

(a) K-means applied on the scattering transforms computed on ultrasonographies

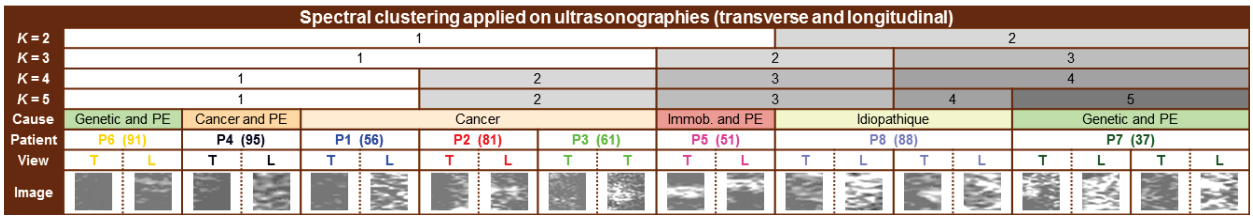

(b) Spectral clustering in K classes computed on ultrasonographies

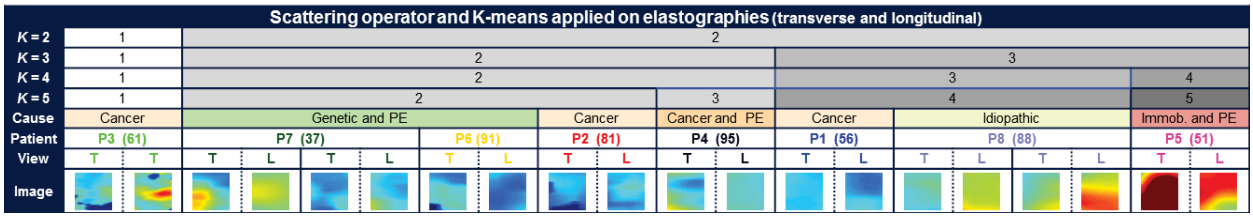

(c) K-means applied on the scattering transforms computed on elastographies

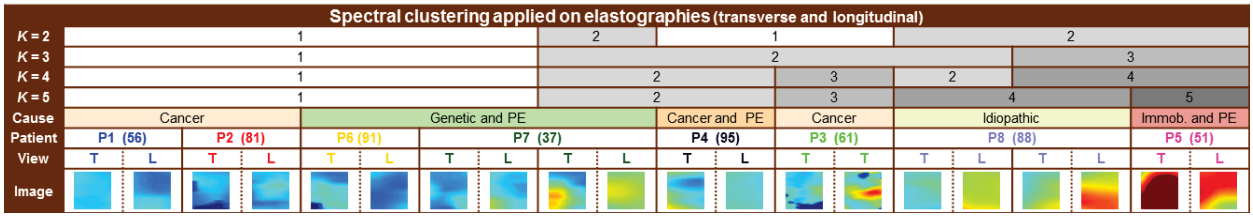

(d) Spectral clustering in K classes computed on elastographies

Fig. 4 Results with Transverse (T) and Longitudinal (L) ultrasound images (the number inside the parenthesis near the patient ID is the patient age)

ACKNOWLEDGMENT

This research project is supported by the Brittany region (Région Bretagne, France) and the French Clinical Research Infrastructure Network on Venous Thrombo-Embolism (F-CRIN INNOVTE). The authors would like also to acknowledge Brest University Hospital, ENSTA Bretagne and Toshiba for their supports.

REFERENCES

[1] R. W. Colman, *Hemostasis and thrombosis: basic principles and clinical practice*. Philadelphia, PA, USA: Lippincott Williams & Wilkins, 2006.

[2] A. T. Cohen, G. Agnelli, F. A. Anderson, J. I. Arcelus, D. Bergqvist, J. G. Brecht, I. A. Greer, J. A. Heit, J. L. Hutchinson, A. Kakkar *et al.*, "Venous thromboembolism (vte) in europe," *Thrombosis and Haemostasis*, vol. 98, no. 4, pp. 756–764, 2007.

[3] J. P. Carpenter, G. A. Holland, R. A. Baum, R. S. Owen, J. T. Carpenter, and C. Cope, "Magnetic resonance venography for the detection of deep venous thrombosis: comparison with contrast venography and duplex doppler ultrasonography," *Journal of vascular surgery*, vol. 18, no. 5, pp. 734–741, 1993.

[4] A. Dahabiah, J. Puentes, B. Guias, L. Bressollette, and B. Solaiman, "Comparative neural network based venous thrombosis echogenicity and echostructure characterization using ultrasound images," in *Information and Communication Technologies, 2006. ICTTA'06. 2nd*, vol. 1. Damascus, Syria: IEEE, 2006, pp. 992–997.

[5] B. Geier, L. Barbera, D. Muth-Werthmann, S. Siebers, H. Ermert, S. Philippou, A. Mumme *et al.*, "Ultrasound elastography for the age determination of venous thrombi evaluation in an animal model of venous thrombosis," *Thrombosis and haemostasis*, vol. 93, no. 2, pp. 368–374, 2005.

[6] E. Mfoumou, J. Tripette, M. Blostein, and G. Cloutier, "Time-dependent hardening of blood clots quantitatively measured in vivo with shear-wave ultrasound imaging in a rabbit model of venous thrombosis," *Thrombosis research*, vol. 133, no. 2, pp. 265–271, 2014.

[7] B. S. Garra, "Elastography: history, principles, and technique comparison," *Abdominal imaging*, vol. 40, no. 4, pp. 680–697, 2015.

[8] T. Berthomier, A. Mansour, L. Bressollette, F. Le Roy, and D. Mottier, "Deep venous thrombosis: Database creation and image preprocessing," in *Frontiers of Signal Processing (ICFSP), International Conference on*. Warsaw, Poland: IEEE, 2016, pp. 87–92.

[9] K. Zuiderveld, "Contrast limited adaptive histogram equalization," in *Graphics Gems IV*, P. S. Heckbert, Ed. San Diego, CA, USA: Academic Press Professional, Inc., 1994, pp. 474–485.

[10] T. Berthomier, A. Mansour, L. Bressollette, F. L. Roy, and D. Mottier, "Deep venous thrombus characterization : ultrasonography ,

elastography and scattering operator," *Advances in Science, Technology and Engineering Systems Journal*, vol. 2, no. 3, pp. 48–59, 2017.

[11] J. Bruna and S. Mallat, "Invariant scattering convolution networks," *IEEE transactions on pattern analysis and machine intelligence*, vol. 35, no. 8, pp. 1872–1886, 2013.

[12] L. Sifre and S. Mallat, "Rotation, scaling and deformation invariant scattering for texture discrimination," in *Proceedings of the IEEE conference on computer vision and pattern recognition*, 2013, pp. 1233–1240.

[13] N. Valeyrie, Y. Pailhas, C. Capus, and Y. Petillot, "Texture recognition in synthetic aperture sonar images with scattering operators," in *4th International Conference and Exhibition on Underwater Acoustic Measurements: Technologies & Results*, 2011.

[14] U. Von Luxburg, "A tutorial on spectral clustering," *Statistics and computing*, vol. 17, no. 4, pp. 395–416, 2007.

[15] D. Hamad and P. Biela, "Introduction to spectral clustering," in *Information and Communication Technologies: From Theory to Applications, 2008. ICTTA 2008. 3rd International Conference on*. Damascus, Syria: IEEE, 2008, pp. 1–6.

[16] N. Archip, R. Rohling, P. Cooperberg, H. Tahmasebpour, and S. Warfield, "Spectral clustering algorithms for ultrasound image segmentation," *Medical Image Computing and Computer-Assisted Intervention–MICCAI 2005*, pp. 862–869, 2005.

[17] P. Chuzel, A. Mansour, J. Ognard, J. Gentric, L. Bressollette, D. Hamad, and N. Betrouni, "Automatic clustering for mri images, application on perfusion mri of brain," in *Frontiers of Signal Processing (ICFSP), International Conference on*. Warsaw, Poland: IEEE, 2016, pp. 63–66.

[18] A. Y. Ng, M. I. Jordan, and Y. Weiss, "On spectral clustering: Analysis and an algorithm," in *Advances in neural information processing systems*, Cambridge, MA, USA, 2002, pp. 849–856.

[19] E. Oyallon and S. Mallat, "Deep roto-translation scattering for object classification," in *Proceedings of the IEEE Conference on Computer Vision and Pattern Recognition*, 2015, pp. 2865–2873.

[20] M. Fritz, E. Hayman, B. Caputo, and J.-O. Eklundh, "The kth-tips database," 2004.

[21] H.-G. Nguyen, R. Fablet, and J.-M. Boucher, "Visual textures as realizations of multivariate log-gaussian cox processes," in *Computer Vision and Pattern Recognition (CVPR), 2011 IEEE Conference on*. IEEE, 2011, pp. 2945–2952.

[22] M. Crosier and L. D. Griffin, "Texture classification with a dictionary of basic image features," in *Computer Vision and Pattern Recognition, 2008. CVPR 2008. IEEE Conference on*. IEEE, 2008, pp. 1–7.

[23] L. Liu, P. Fieguth, G. Kuang, and H. Zha, "Sorted random projections for robust texture classification," in *Computer Vision (ICCV), 2011 IEEE International Conference on*. IEEE, 2011, pp. 391–398.

[24] X. Deng, Q. Liu, Y. Deng, and S. Mahadevan, "An improved method to construct basic probability assignment based on the confusion matrix for classification problem," *Information Sciences*, vol. 340, pp. 250–261, 2016.

[25] T. Berthomier, A. Mansour, L. Bressollette, F. Le Roy, and D. Mottier, "Venous blood clot structure characterization using scattering operator," in *Frontiers of Signal Processing (ICFSP), International Conference on*. Warsaw, Poland: IEEE, 2016, pp. 73–80.